**Electronic Supplementary Material_1**

**Title:** Sub-region-specific optic nerve head glial activation in glaucoma.


**Authors**

Kazuya Oikawa[1, 2, 3], James N. Ver Hoeve[2, 3], Leandro B.C. Teixeira[3, 4], Kevin C. Snyder[1, 3], Julie A. Kiland[2], N. Matthew Ellinwood[5], Gillian J. McLellan[1, 2, 3*]

1. Department of Surgical Sciences, University of Wisconsin-Madison, Madison, WI, USA.

2. Department of Ophthalmology and Visual Sciences, University of Wisconsin-Madison, Madison, WI, USA.

3. McPherson Eye Research Institute, Madison, WI, USA

4. Department of Pathobiological Sciences, University of Wisconsin-Madison, Madison, WI, USA

5. Department of Animal Science, Iowa State University, Ames, IA, USA

*Corresponding author

Gillian J. McLellan

1300 University Avenue

Madison, WI 53706

+1 (608) 265 9848

gillian.mclellan@wisc.edu

**Supplemental materials and methods**

**Electrophysiological Testing**: Electrophysiological testing was performed using the UTAS Visual Diagnostic System (LKC Technologies, Gaithersburg, MD) to record full-field ERG and VEP responses. In all subjects, two test sessions were conducted at least one week apart, with responses for the two testing sessions averaged. All testing was performed under ketamine-xylazine anesthesia. Topical 2% dorzolamide was applied to eyes of FCG cats 1-2 hours prior to testing to prevent acute IOP elevation due to pharmacologic mydriasis (1), the latter achieved with topical 1% tropicamide instilled 20 minutes prior to testing. Topical anesthetic (0.5% proparacaine) was applied immediately prior to testing. Data were only collected when IOP values were lower than 40 mmHg at the time of testing (2). Heart rate, respiration rate, $SpO_2$, and body temperature were monitored, and maintained within normal physiological range during each recording session. ERG Jet corneal electrodes (Fabrinal SA, La Chaux-De-Fonds, Switzerland) were referenced to subdermal needle electrodes placed in the periocular skin adjacent to and 2 cm posterior to the lateral canthus. Photopic flash ERGs were recorded in response to a sequence of 8 increasing intensity steps ranging from 0.007 cd-s/$m^2$ to 10.75 cd-s/$m^2$, averaging 5 sweeps for each response. Peak amplitudes and implicit times of a- and b-waves were scored automatically using a custom automated analysis algorithm (Matlab, Mathworks, Natick, MA), and intensity response function (Naka-Rushton) plotted for b-wave amplitudes. Cortical VEP responses were recorded in duplicate from sub-dermal needle electrodes overlying the right and left occipital cortices to 4.1 Hz white flashes (2.7 cd-s/$m^2$ on a white 30 cd/$m^2$ background). Monocular stimuli were presented, by occlusion of each eye in turn, averaging 80 sweeps per trial. Simultaneous collection of ERGs from both eyes verified effective monocular occlusion and absence of ERG contamination of VEP responses. Root mean square of VEP amplitudes of the early wavelets (RMS) (0 - 35 msec implicit time) and peak amplitudes and latencies of the late positive component (designated P2) of VEPs were calculated and averaged over two sessions, using a custom automated analysis algorithm (Matlab, Mathworks, Natick, MA).

**Quantification of Optic Nerve Axons.** Optic nerve axons were quantified following a published protocol that has been validated for feline normal and glaucomatous optic nerves (3). Briefly, 2mm portions of orbital, retrobulbar optic nerve were fixed in 4% paraformaldehyde in 0.1M PBS at 4 °C overnight, then transferred to 0.1M PBS at 4°C prior to further processing. Nerve samples were post-fixed in 2.5% glutaraldehyde/0.1 M PBS for 48 h at 4°C; osmicated in 1% osmium tetroxide in 0.1M PBS; rinsed, and dehydrated through an ascending series of alcohol concentrations before routine epoxy resin embedding and semi-thin (1μm) sectioning. Coronal sections were stained with Richardson's stain and with 1% p-phenylenediamine (PPD) for light microscopy and histomorphometry using commercially available image analysis software (cellSens Dimension®, Olympus Inc.).

**RNA Extraction**. Total RNA was extracted under RNase free conditions from ONH tissue using RNeasy Fibrous Tissue Mini Kit (Qiagen, Germantown, MD), following homogenization in RLT buffer reagent by Tissue Ruptor® (Qiagen), according to the manufacturer's instructions. Concentration of RNA for each sample was determined by Qubit® 2.0 fluorometer (Invitrogen). RNA quantity and quality were assessed by Nanodrop® ND-1000 spectrophotometer (Thermo Scientific) determining 260/280nm and 260/230nm absorption ratios. Additionally, an RNA integrity number (RIN) and electropherogram were evaluated by Bioanalyzer 2100 (RNA 6000 pico chip; Agilent Technologies, Palo Alto, CA). Only samples with RIN ≥ 8, distinct 28S rRNA and 18S rRNA peaks on electropherogram, and RNA quantity ≥ 150ng were included in downstream applications in this study.

**Library Construction and RNA sequencing**: Each RNA library was generated using a paired-end, strand-specific approach following the Illumina TruSeq® Stranded mRNA Sample Preparation Guide Rev.E. The Poly-A containing mRNA was purified from 150-500ng total RNA. Quality and quantity

of the libraries were validated using Bioanalyzer 2100 (Agilent DNA1000 chip; Agilent Technologies, Santa Clara, CA) and Qubit® 2.0 fluorometer (dsDNA HS Kit; Invitrogen, Carlsbad, CA), respectively. Each library was multiplexed for 2x100bp sequencing using the TruSeq 100bp SBS kit (v3) and sequenced by Illumina® HiSeq2000 (illumina, San Diego, CA).

***RNA-seq alignment, expression estimation, and differential expression analysis***.

Generated raw reads (FASTQ format) were quality-control checked by FastQC (4) after filtering to remove adaptor sequences, low-quality reads (quality score <20) and those that did not meet filter length ( length <28) by Skewer (ver 0.1.127) (5), a fast and sensitive adapter trimmer for Illumina paired-end sequences. Mapping of trimmed reads to the *Felis catus* reference genome sequence (ICGSC Felis_catus_8.0/ felCat8) was performed using STAR ver 2.4.2a (6). A total of 775.8 million raw paired-end reads (average 48.5 million raw paired-end reads per sample) were generated, and 761.9 million trimmed paired reads (average 47.6 million paired reads per sample) were used in further analyses after quality filtering. The average proportion of uniquely mapped reads to the Felis catus reference genome was 91.88%. Gene transcript abundances were estimated by RSEM ver 1.2.22 (7). RSEM generated the following values: expected counts, transcripts per million (TPM), and the fragments per kilobase of exon per million reads mapped (FPKM). Based on the model assumption that gene counts follow negative binominal distribution, differential expression (DE) analyses between normal and glaucomatous biological conditions were performed using DEseq2 ver.1.10.0 (8), edgeR ver 3.13.4 (9), and EBseq ver.1.11.1 (10). DEGs between groups were considered significant with FDR < 0.05.

**Functional Enrichment Analysis.** Enrichment in molecular pathways and GO terms were assigned using the Database for Annotation, Visualization and Integrated Discovery (DAVID, ver.6.8) (11) and Blast2GO (ver.3.3) (12), respectively. The DAVID was used to add functional annotation to gene

lists, and pathways in KEGG (13) were used for enrichment analysis in DAVID. Blast2GO, designed for the purpose of enabling GO term (14) biological processes -based data mining, utilized sequence data by homology. Default Blast expectation values (E-value; set at $< 10^{-10}$) and hit number threshold (set at 10) were applied to retrieve significant results. Two-tailed Fisher's exact test with Benjamini-Hochberg correction was used to identify statistically over-represented GO terms, with FDR <0.05. Enriched GO terms often have parent-child relationships and therefore mask more specific biological processes if only the degree of statistical significance is considered. Thus, the "Reduce to most specific terms" function in the software was used to identify the most specific but significant GO terms.

**WGCNA:** WGCNA is a co-expression network analysis that has been widely used in large transcriptome datasets (15). A signed co-expression network was constructed using R package WGCNA (ver. 1.47). FPKM values were filtered (lower threshold FPKM < 1) and then normalized by log2(FPKM+1) transformation. In total, 12,095 genes were included in the network analysis. A pair-wise correlation matrix, also known as an adjacency matrix, was computed by calculating the bi-weight mid-correlation. This adjacency matrix was then raised to a soft threshold power of 6 to achieve a scale-free topology. For each pair of genes, a robust measure of network interconnectedness (topological overlap measure: TOM) was calculated based on the adjacency matrix. The TOM-based dissimilarity was then used as input for average linkage unsupervised hierarchical clustering. To cut the branches, hybrid dynamic tree cutting was used because it leads to robustly defined modules. Minimum module size was set to 25 genes and the minimum height for merging modules was set at 0.2. The TOM was calculated for the genes in each module ranked. The resulting list of gene pairs was filtered so that both genes in a pair had the highest module membership for the module plotted. Gene modules were formed by unsupervised clustering of genes by hierarchical clustering based on the threshold of dissimilarity, 1-TOM. The hub genes in upper quartile in the modules were visualized using Cytoscape ver 3.3 (16) and Enrichment map Cytoscape plug-in (17).

**RT-qPCR**: Total RNA was reverse transcribed to cDNA with oligo (dT) 15 primers and SuperScript™ III Reverse Transcriptase (ThermoFisher Scientific). The total RNA concentration was determined using a Qubit® 3.0 fluorometer (RNA HS Kit; Invitrogen, Carlsbad, CA). The cDNA was added to diluted SYBR Green PCR master mix (Applied Biosystems, Grand Island, NY) with 0.25 µM of each primer in a 20 µl reaction volume. Each cDNA sample (biological replicates: 5 early FCG and 4 age-matched controls) was run in triplicate on QuantStudio™ 7 Flex Real-time PCR system (Applied Biosystems, Grand Island, NY). Quantitative PCR was performed for 5 DEGs (*LGALS3*, *HP*, *UPK1B*, *NMNAT2* and *RYR1*) and a reference gene *TBP* (18) using the primer sequences listed in Supplemental table 5. PCR cycling conditions were 95 °C (15 s) and 60 °C (60 s) for 40 cycles. PCR products were confirmed by gel electrophoresis. For relative quantification, the $2^{-\Delta Ct}$ method was used, implemented in Expression Suite software v 1.1 (ThermoFisher Scientific). For each target, a standard curve was established to confirm that PCR efficiency was between 95% and 105%. Water was substituted for cDNA in non-template controls and template known to express target genes was used as positive control. Data were normalized to *TBP* expression for each sample.

**Supplemental Table S1.**

Publicly available genesets for cell-type specific and microglial molecular signature in the GSEA analyses.

| Source (reference) | Geneset |
|---|---|
| Gupta S et al. (2014) (19) | Astrocytes, Oligodendrocyte, Synaptic proteins |
| Cahoy JD et al. (2008) (20) | Astrocytes, Neurons, OPC and Oligodendrocytes |
| Zhang Y et al. (2014) (21) | Astrocytes, Neurons, Microglia and Oligodendrocytes |
| Hirbec H et al. (2018) (22) | LPS activated microglia |
| Sousa C et al. (2018) (23) | LPS activated microglia |
| Holtman IR et al. (2015) (24) | Microglia molecular signature associated aging and acute LPS responses |
| Friedman BA et al. (2018) (25) | Neurodegeneration-related microglia |
| Karen-Shaul H et al. (2017) (26) | Damage-associated microglia (DAM) |
| Hammond TR et al. (2018) (27) | Aging related microglia signature |

**Supplemental Table S2. Primary antibodies used in this study.**

| Antibody | Catalog # | Supplier | Host | Clonality | Dilution | RRID |
|---|---|---|---|---|---|---|
| IBA1 | 019-19741 | Wako | Rabbit | Polyclonal | 1:200 | AB_839504 |
| OLIG2 | AB9610 | Millipore | Rabbit | Polyclonal | 1:500 | AB_570666 |
| Ki-67 | M7240 | DAKO | Mouse | Monoclonal | 1:200 | AB_2142367 |
| SOX2 | sc-17320 | Santa Cruz Biotechnology | Goat | Polyclonal | 1:200 | AB_2286684 |
| GFAP | 13-0300 | ThermoFisher Scientific | Rat | Polyclonal | 1:2000 | AB_2532994 |
| P2RY12 | NBP2-33870 | Novus Biologicals | Rabbit | Polyclonal | 1:1500 | AB_2810254 |
| IBA1 | NB 100-1028 | Novus Biologicals | Goat | Polyclonal | 1:1500 | AB_521594 |

**Supplemental Table S3. Top 15 up-regulated, differentially expressed genes in the ONH in early FCG relative to normal controls.**

| Gene | Description | Log2 (fold-change) | *P*-value | FDR |
|---|---|---|---|---|
| *DMRT2* | Doublesex and mab-3 related transcription factor 2 | 1.62 | 3.61E-08 | 1.29E-04 |
| *HP* | Haptoglobin | 1.59 | 5.97E-09 | 5.33E-05 |
| *SPTA1* | Spectrin, alpha, erythrocytic 1 | 1.55 | 3.54E-08 | 1.29E-04 |
| *UPK1B* | Uroplakin 1B | 1.47 | 2.04E-07 | 3.14E-04 |
| *PRG4* | Proteoglycan 4 | 1.44 | 1.56E-07 | 3.09E-04 |
| *E2F8* | E2F transcription factor 8 | 1.30 | 7.06E-07 | 5.46E-04 |
| *APOPT1* | Apoptogenic 1, mitochondrial | 1.30 | 2.11E-06 | 1.18E-03 |
| *SLC16A4* | Solute carrier family 16, member 4 | 1.25 | 1.02E-06 | 7.25E-04 |
| *LGALS3* | Lectin, galactoside-binding, soluble, 3 | 1.21 | 6.08E-07 | 5.42E-04 |
| *CXCL6* | Alveolar macrophage chemotactic factor | 1.19 | 1.76E-05 | 4.70E-03 |
| *CD14* | CD14 molecule | 1.18 | 2.72E-06 | 1.31E-03 |
| *CCR2* | Chemokine (C-C motif) receptor 2 | 1.17 | 9.64E-06 | 3.13E-03 |
| *APOA2* | Apolipoprotein A-II | 1.17 | 7.38E-05 | 1.15E-02 |
| *RFPL4B* | Ret finger protein-like 4B | 1.15 | 9.35E-05 | 1.29E-02 |
| *MGP* | Matrix Gla protein | 1.15 | 8.25E-05 | 1.22E-02 |

**Supplemental Table S4. Top 15 down-regulated, differentially expressed genes in the ONH in early FCG relative to normal controls.**

| Gene | Description | Log2 (fold-change) | *P*-value | FDR |
|---|---|---|---|---|
| *ARHGAP36* | Rho GTPase activating protein 36 | -1.52 | 2.16E-07 | 3.14E-04 |
| *CD1B* | CD1b molecule | -1.35 | 2.70E-06 | 1.18E-03 |
| *SYNDIG1L* | Synapse differentiation inducing 1-like | -1.35 | 2.09E-06 | 5.46E-04 |
| *BAAT* | Bile acid-CoA:amino acid N-acyltransferase | -1.31 | 6.74E-07 | 3.14E-04 |
| *CD1C* | T-cell surface glycoprotein CD1c | -1.31 | 4.40E-06 | 1.83E-03 |
| *KRT35* | Keratin 35, type I | -1.23 | 3.31E-05 | 6.66E-03 |
| *SLC14A1* | Solute carrier family 14 (urea transporter), member 1 (Kidd blood group) | -1.21 | 6.09E-06 | 2.27E-03 |
| *TMEM176A* | Transmembrane protein 176A | -1.10 | 2.25E-05 | 5.49E-03 |
| *TMEM176B* | Transmembrane protein 176B | -1.09 | 3.31E-05 | 6.66E-03 |
| *SMIM17* | Small integral membrane protein 17 | -1.09 | 2.59E-06 | 1.31E-03 |
| *BST2* | Bone marrow stromal cell antigen 2 | -1.07 | 5.47E-05 | 9.34E-03 |
| *GRIN2B* | Glutamate receptor, ionotropic, N-methyl D-aspartate 2B | -1.06 | 4.26E-05 | 7.67E-03 |
| CD300E | CMRF35-like molecule 2 | -1.05 | 4.01E-04 | 3.00E-02 |
| CCDC37 | Coiled-coil domain containing 37 | -1.01 | 3.72E-04 | 2.85E-02 |
| ZCCHC13 | Zinc finger, CCHC domain containing 13 | -0.99 | 7.86E-04 | 4.28E-02 |

**Supplemental Table S5. Primers used in RT-qPCR experiments to validate RNA-seq results**.

| Gene name | | Primer sequence (5' – 3') | Primer length | Size (bp) |
|---|---|---|---|---|
| *TBP* | Forward | TTC GTG CCC GAA ATG CTG AA | 20 | 135 |
| | Reverse | ACT GCT CTT CAC TCT TGG CTC | 21 | 135 |
| *RYR1* | Forward | CTG CGA AGA GGG CTA TGT GA | 20 | 83 |
| | Reverse | CGG CGG AAA TGG TAA GAC AC | 20 | 83 |
| *LGALS3* | Forward | ACT GTG CCT TAT GAC CTG CC | 20 | 97 |
| | Reverse | AAG CAA GTC TGT TTG CAT TGG G | 22 | 97 |
| *HP* | Forward | CCA AAG CCC CCA GAG ATT GA | 20 | 176 |
| | Reverse | TTT CCG CAC ACT GCT TCA CA | 20 | 176 |
| *UPK1B* | Forward | GCC TGT CCG TTC TAG GCA TT | 20 | 145 |
| | Reverse | TTG GGC GTG AAA AAG TCT CG | 20 | 145 |
| *NMNAT2* | Forward | CGC AAG ATG ACG GAG ACC AC | 20 | 102 |
| | Reverse | CCT GGC TCT TTC GAA CAT CTG | 21 | 102 |

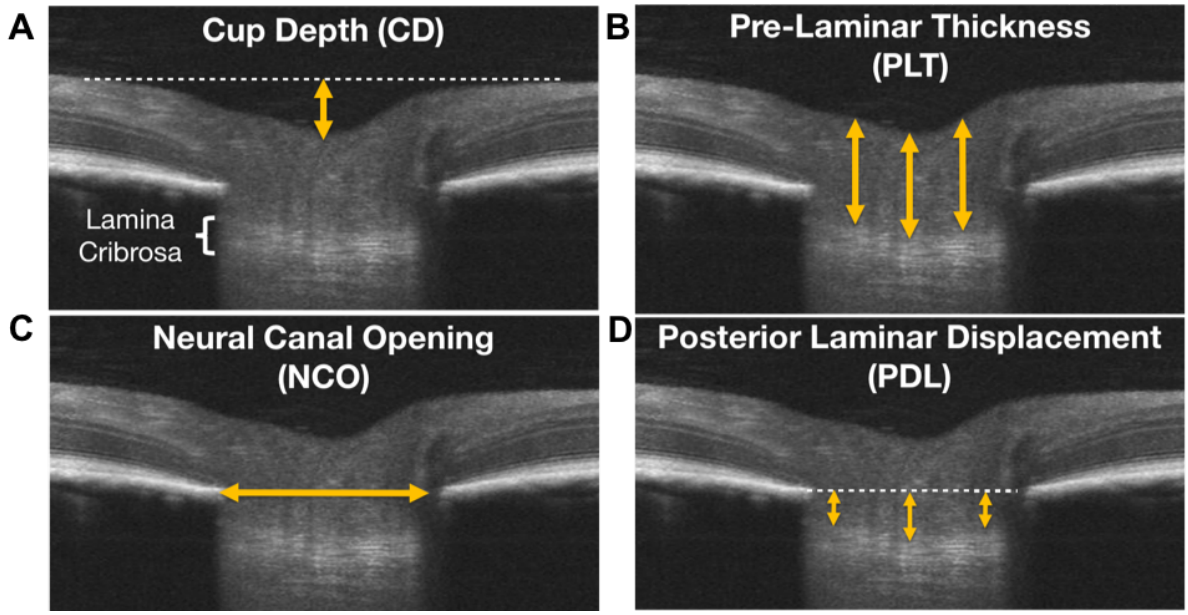


**Supplemental Figure S1. Illustration of parameters measured in Optical Coherence Tomography Images of Feline Optic Nerve Head (ONH)**

Yellow arrows depict: (**A**) Cup depth (CD), which is measured as the distance between a horizontal line at the level of the internal limiting membrane of the retina (dotted white line) and the deepest part of the anterior surface of the optic nerve head; (**B**) Pre-laminar tissue thickness (PLT), defined as the distance between the internal limiting membrane surface and the anterior laminar surface; (**C**) Neural canal opening (NCO), measured as a line drawn between the reflections at the ONH margins consistent with Bruch's membrane opening, and (**D**) Posterior laminar displacement (or "posterior displacement of the lamina" [PDL]) represents the mean distance measured vertically between a horizontal line extending across the neural canal opening and the anterior laminar surface.

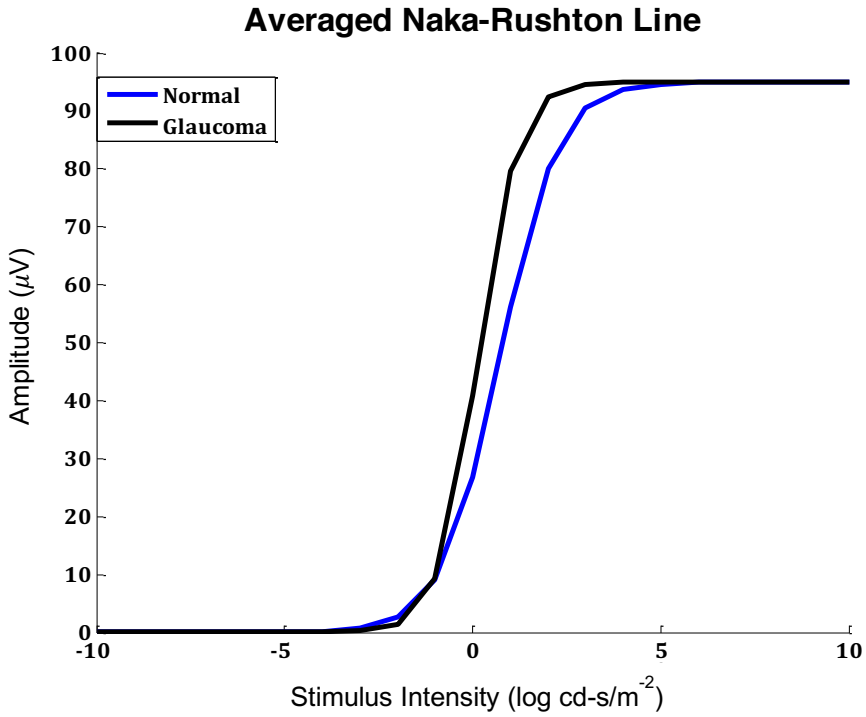


**Supplemental Figure S2. Intensity-response function of the photopic ERG was not significantly different from normal age matched subjects in feline congenital glaucoma**

Electroretinogram (ERG) was recorded concurrently with visual evoked potential (VEP) and amplitudes of ERG b waves were plotted against stimulus intensity and fit with the Naka-Rushton equation. A slight, and statistically insignificant "left shift" in the intensity-response curve was identified in subjects with FCG compared to normal controls, suggesting that VEP functional abnormalities detected are not attributable to photoreceptor and/or bipolar cell dysfunction.

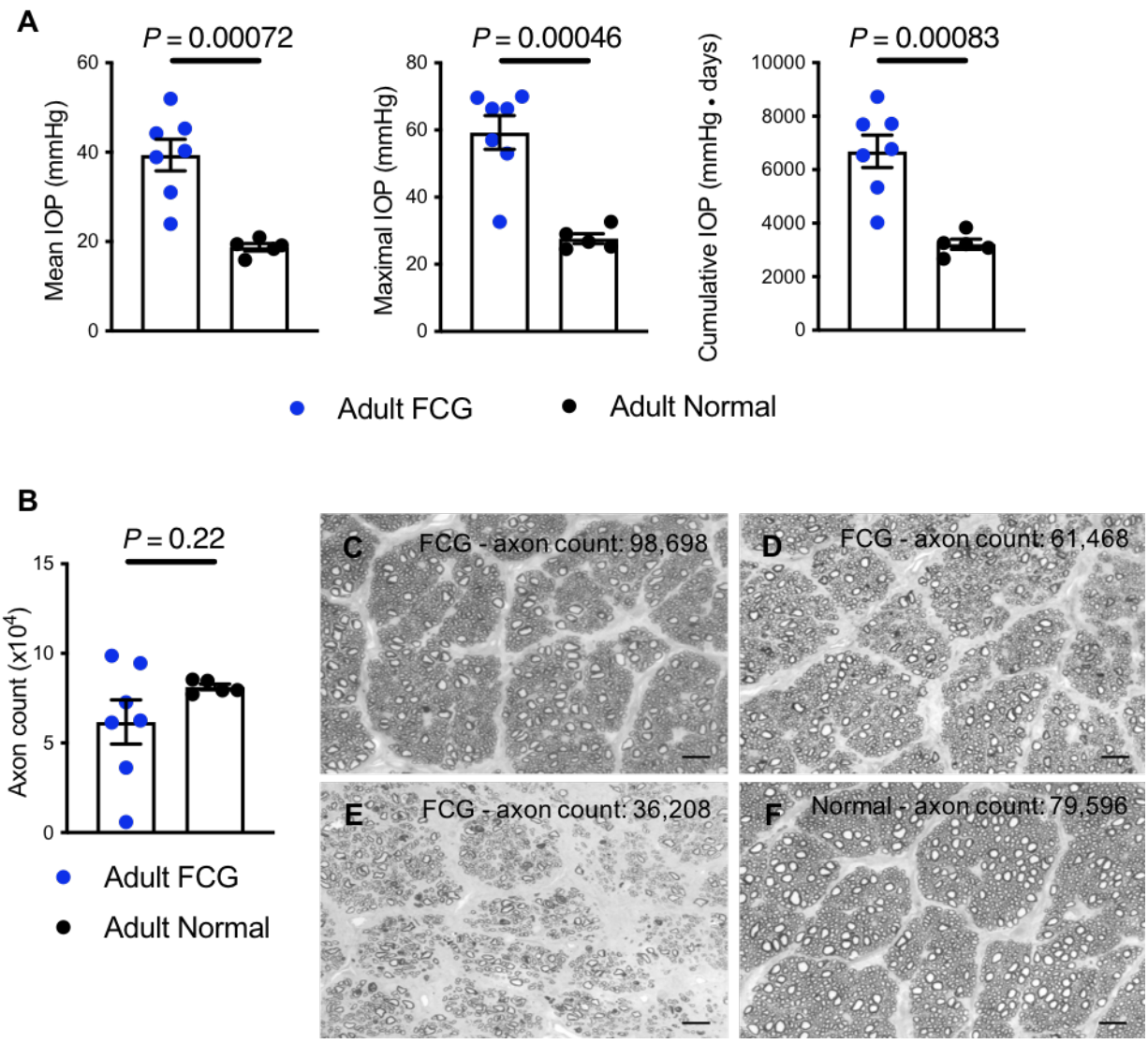


**Supplemental Figure S3. Chronic elevation of IOP and variable degrees of optic nerve damage in a cohort of young adult cats with FCG**

(**A**) Mean, maximal and cumulative intraocular pressure (IOP), collected weekly over the 6 months prior to euthanasia, were significantly and consistently higher in 1-2 year-old young adult FCG than in age-matched normal subjects. (**B**) Optic nerve axon count and p-phenylenediamine stained optic nerve cross sections in adult FCG (**C**-**E**) demonstrate various degrees of optic nerve injury compared to age-matched control (**F**), reflecting intra-individual variability in optic nerve damage in this adult feline cohort, randomly selected from a large tissue archive based solely on age (1-2 year-old). Scale

bar = 20 μm. Mean and SEM are presented; all comparisons between normal ($n$ = 5) and FCG ($n$ = 6) were by unpaired 2-tailed t-test.

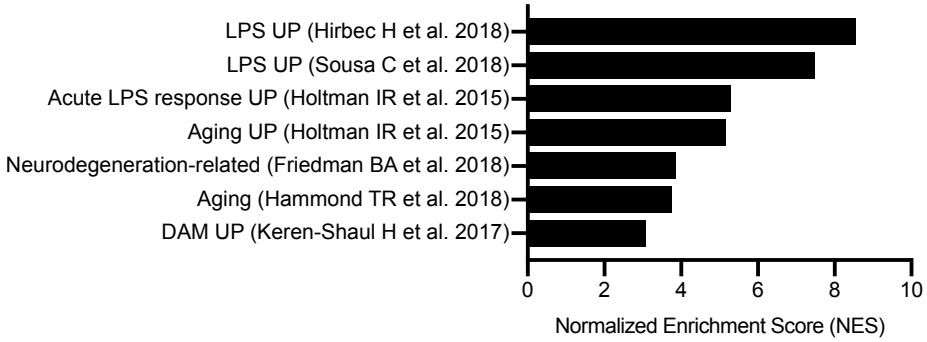


**Supplemental Figure S4. Early glaucomatous ONH transcriptome is enriched with pro-inflammatory, LPS-stimulated microglia molecular signatures.**

GSEA results depicted in this bar graph demonstrate that the ONH transcriptome in early FCG is most highly enriched for the LPS-activated microglia genesets, among other microglia molecular phenotypes tested including the disease associated microglia (DAM) signature. The genesets were retrieved from published gene expression datasets for distinct microglial molecular phenotypes.

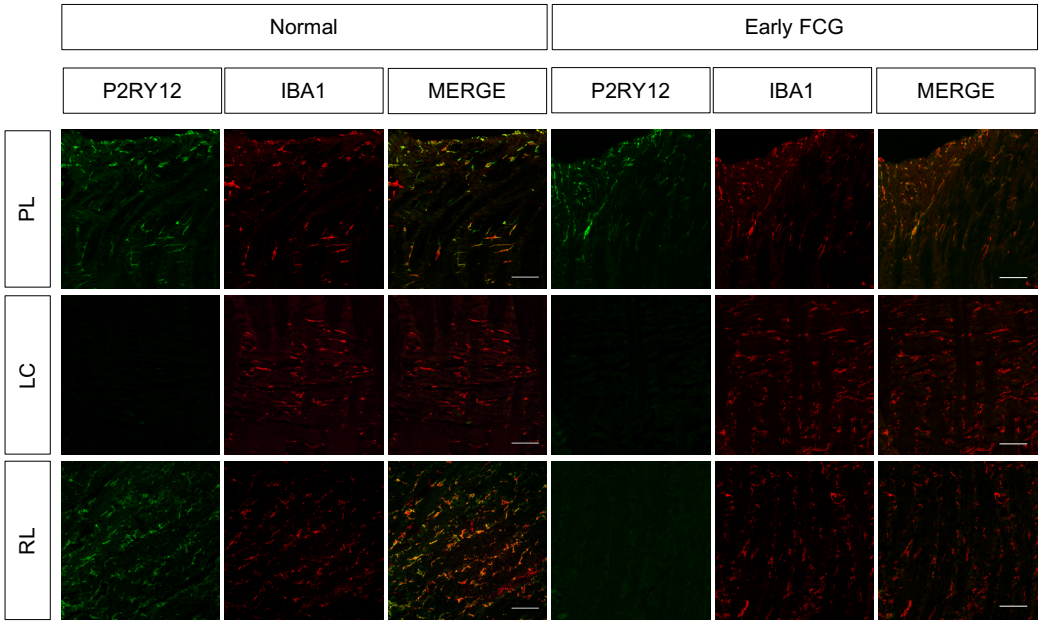


**Supplemental Figure S5. Expression of P2RY12 in IBA1$^+$ cells in the ONH**

Representative immunofluorescent photomicrographs of ONH tissues from a 11-week-old cat with early FCG and an age-matched normal cat showing expression of P2RY12 (green; microglia specific marker) and IBA1 (red; myeloid cell marker) in each sub-region of the ONH. In normal feline ONH, P2RY12 is expressed in the majority of IBA$^+$ cells in the PL and RL regions, but not in the LC region. While P2RY12 is similarly co-expressed in IBA$^+$ cells in the PL region in the glaucomatous ONH, P2RY12 expression is lower in the ONH RL region in early FCG than in the age-matched normal control. Scale bar = 25 μm.

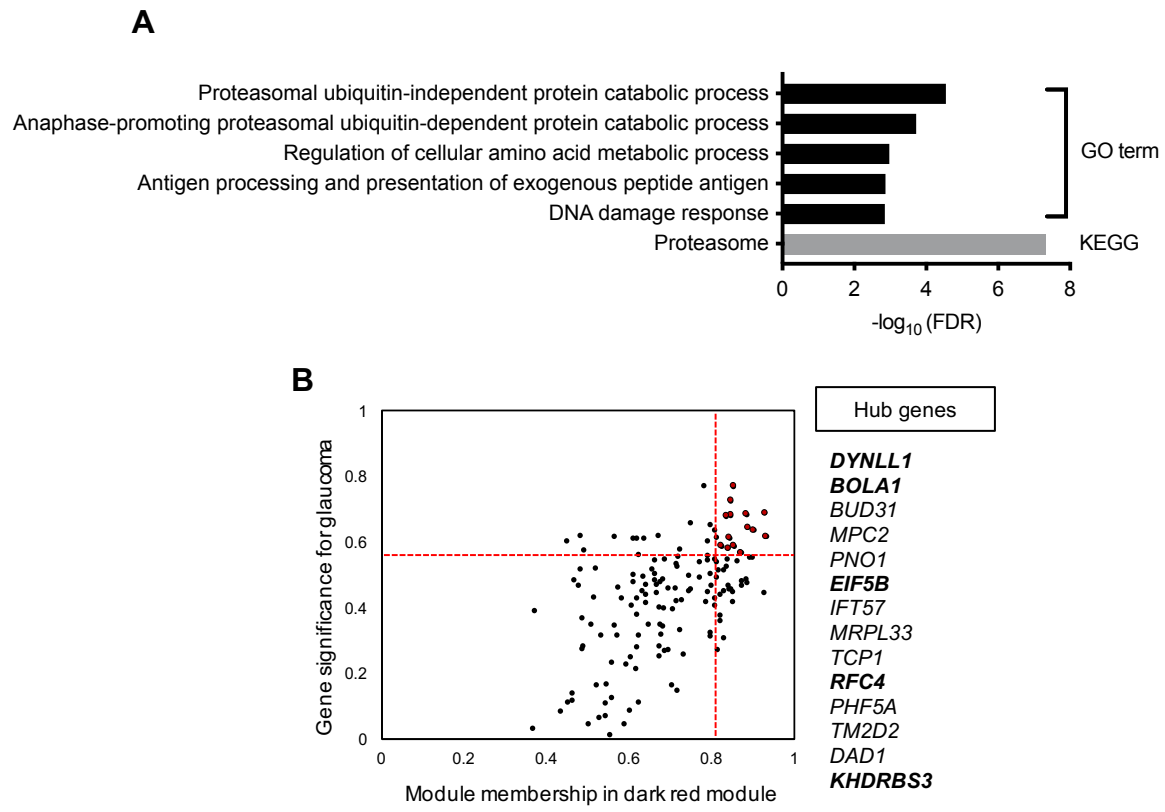


**Supplemental Figure S6. The darkred module associated with glaucoma genotype and IOP is enriched with proteasome-related pathways.**

**(A)** The top five over-represented GO terms in the "darkred" module and the over-represented KEGG pathway are shown. Genes associated with proteasomal ubiquitin-independent protein catabolic processes (FDR< $2.85 \times 10^{-5}$) and proteasome (FDR < 0.05) are over-expressed in early glaucoma in the FCG model. (**B**) Scatter plot demonstrates module membership and gene significance in the darkred modules for FCG. Each dot represents a single gene in the modules (151 genes). Genes that have high module membership (vertical red line; upper quartile) and high gene significance for glaucoma (horizontal red line; upper quartile) are considered hub genes (red dots). The hub genes listed on the right (bold), are hub genes in both genotype and IOP.

**Supplemental References:**

1. Gomes FE, Bentley E, Lin T-L, McLellan GJ. Effects of unilateral topical administration of 0.5% tropicamide on anterior segment morphology and intraocular pressure in normal cats and cats with primary congenital glaucoma.. *Vet Ophthalmol* 2011;14 Suppl 1:75–83.

2. Siliprandi R, Bucci MG, Canella R, Carmignoto G. Flash and pattern electroretinograms during and after acute intraocular pressure elevation in cats.. *Investigative Ophthalmology & Visual Science* 1988;29(4):558–565.

3. Teixeira LBC et al. Quantifying optic nerve axons in a cat glaucoma model by a semi-automated targeted counting method. *Mol. Vis.* 2014;20:376–385.

4. Andrew S. FastQC: a quality control tool for high throughput sequence data2010;

5. Jiang H, Lei R, Ding S-W, Zhu S. Skewer: a fast and accurate adapter trimmer for next-generation sequencing paired-end reads. *BMC Bioinformatics* 2014;15(1):182.

6. Dobin A et al. STAR: ultrafast universal RNA-seq aligner. *Bioinformatics* 2012;29(1):15–21.

7. Li B, Dewey CN. RSEM: accurate transcript quantification from RNA-Seq data with or without a reference genome. *BMC Bioinformatics* 2011;12(1):323.

8. Love MI, Huber W, Anders S. Moderated estimation of fold change and dispersion for RNA-seq data with DESeq2. *Genome Biol.* 2014;15(12):550–21.

9. Robinson MD, McCarthy DJ, Smyth GK. edgeR: a Bioconductor package for differential expression analysis of digital gene expression data. *Bioinformatics* 2009;26(1):139–140.

10. Leng N et al. EBSeq: an empirical Bayes hierarchical model for inference in RNA-seq experiments.. *Bioinformatics* 2013;29(8):1035–1043.

11. Huang DW, Sherman BT, Lempicki RA. Systematic and integrative analysis of large gene lists using DAVID bioinformatics resources. *Nat Protoc* 2008;4(1):44–57.

12. Conesa A et al. Blast2GO: a universal tool for annotation, visualization and analysis in functional genomics research. *Bioinformatics* 2005;21(18):3674–3676.

13. Kanehisa M, Goto S. KEGG: kyoto encyclopedia of genes and genomes.. *Nucl. Acids Res.* 2000;28(1):27–30.

14. The Gene Ontology Consortium. Gene Ontology Consortium: going forward. *Nucl. Acids Res.* 2015;43(D1):D1049–D1056.

15. Langfelder P, Horvath S. WGCNA: an R package for weighted correlation network analysis. *BMC Bioinformatics* 2008;9(1):559.

16. Shannon P. Cytoscape: A Software Environment for Integrated Models of Biomolecular Interaction Networks. *Genome Res.* 2003;13(11):2498–2504.

17. Merico D, Isserlin R, Stueker O, Emili A, Bader GD. Enrichment Map: A Network-Based Method for Gene-Set Enrichment Visualization and Interpretation. *PLoS ONE* 2010;5(11):e13984-12.

18. Aithal MGS, Rajeswari N. Validation of housekeeping genes for gene expression analysis in glioblastoma using quantitative real-time polymerase chain reaction.. *Brain Tumor Res Treat* 2015;3(1):24–29.

19. Gupta S et al. Transcriptome analysis reveals dysregulation of innate immune response genes and neuronal activity-dependent genes in autism. *Nat Commun* 2014;5(1):1206.

20. Cahoy JD et al. A Transcriptome Database for Astrocytes, Neurons, and Oligodendrocytes: A New Resource for Understanding Brain Development and Function. *J. Neurosci.* 2008;28(1):264–278.

21. Zhang Y et al. An RNA-Sequencing Transcriptome and Splicing Database of Glia, Neurons, and Vascular Cells of the Cerebral Cortex. *J. Neurosci.* 2014;34(36):11929–11947.

22. Hirbec H et al. The microglial reaction signature revealed by RNAseq from individual mice.. *Glia* 2018;66(5):971–986.

23. Sousa C et al. Single-cell transcriptomics reveals distinct inflammation-induced microglia signatures.. *EMBO Rep.* 2018;19(11):e46171.

24. Holtman IR et al. Induction of a common microglia gene expression signature by aging and neurodegenerative conditions: a co-expression meta-analysis.. *Acta Neuropathol Commun* 2015;3(1):31.

25. Friedman BA et al. Diverse Brain Myeloid Expression Profiles Reveal Distinct Microglial Activation States and Aspects of Alzheimer's Disease Not Evident in Mouse Models.. *Cell Rep* 2018;22(3):832–847.

26. Keren-Shaul H et al. A Unique Microglia Type Associated with Restricting Development of Alzheimer's Disease.. *Cell* 2017;169(7):1276-1290.e17.

27. Hammond TR et al. Single-Cell RNA Sequencing of Microglia throughout the Mouse Lifespan and in the Injured Brain Reveals Complex Cell-State Changes. *Immunity* 2019;50(1):253-271.e6.